Spectroscopic and Functional Characterization of a Ligand Coordination Mutant of Soybean Lipoxygenase-1: First Coordination Sphere Analogue of Human 15-Lipoxygenase

Theodore R. Holman,*,† Jing Zhou,‡ and Edward I. Solomon*,‡

Contribution from the Department of Chemistry, Stanford University, Stanford, California 94305, and Department of Chemistry and Biochemistry, University of California, Santa Cruz, California 95064

Received August 10, 1998

Abstract: Lipoxygenases are an important class of non-heme iron enzymes which catalyze the hydroperoxidation of unsaturated fatty acids. This study utilizes a combination of electron paramagnetic resonance (EPR), magnetic circular dichroism (MCD), and variable-temperature, variable-field (VTVH) MCD to probe the ground state and excited states of the active site of an iron coordination mutant of soybean lipoxygenase-1 (SLO-1), N694H, and relate the structural modifications with kinetic changes. The sixth coordination ligand for SLO-1, Asn_{694}, is proposed to be a primary factor in the coordination flexibility of the site and is reflected in both its ferrous MCD and ferric EPR spectroscopic properties. In the present study, we compare the spectroscopic properties of the N694H SLO-1 mutant with those of wild-type (WT) SLO-1 and WT human 15-lipoxygenase (15-HLO) and determine that its properties are intermediate between the WT enzymes. WT 15-HLO has a His substitution in the Asn_{694} equivalent position. The low-temperature MCD of the ferrous N694H SLO-1 shows that the site is 6-coordinate (6C), as in 15-HLO; however, the VTVH MCD is more similar to WT SLO-1, with a positive zero field splitting. The low-temperature EPR of ferric N694H SLO-1 exhibits a signal of intermediate rhombicity with an E/D of 0.08, which is intermediate between those for WT SLO-1 (axial, $E/D \approx 0.01$) and 15-HLO (rhombic, $E/D \approx 0.33$). This intermediate spectroscopic behavior can be rationalized by the stronger ligation of the His compared to the Asn; however, since the site in WT SLO-1 is not optimized for His, it does not ligate the iron as strongly as in the human enzyme. The H544N 15-HLO mutant was also expressed; however, it does not bind iron for activity. The kinetics of N694H SLO-1 are also intermediate ($k_{cat} \approx 10 \pm 2\ s^{-1}$) between those for SLO-1 ($k_{cat} \approx 280 \pm 8\ s^{-1}$) and HLO ($k_{cat} \approx 6.2 \pm 0.1\ s^{-1}$), which suggests that this ligand's interaction with the iron center may regulate the enzymatic activity. We propose that this occurs through a change in reduction potential, which in turn affects the hydrogen atom abstraction step in the reaction mechanism.

Introduction

Lipoxygenases (LOs) are a class of non-heme iron dioxygenases which catalyze the incorporation of dioxygen into 1,4-*cis*,*cis*-pentadiene-containing fatty acids (e.g., linoleic and arachidonic acids) to form hydroperoxide products. LOs are widely distributed throughout the plant and animal kingdoms.[1−6] In mammals, three major types of LOs have been identified, inserting dioxygen at the C-5, C-12, and C-15 positions of arachidonic acid. These LO isozymes produce leukotrienes and lipoxins, which are an important family of signaling molecules that mediate a number of biological processes, such as asthma, atherosclerosis, psoriasis, and inflammatory bowel disease.[7,8] In plants, LOs are involved in immunity, growth regulation, and germination.[9,2]

Lipoxygenase contains an essential iron atom which is isolated in the inactive, ferrous oxidation state. The enzyme is activated by 1 equiv of hydroperoxide product ((9*Z*,11*E*)-13-hydroperoxy-9,11-octadecadienoic acid (13-HPOD)) which oxidizes the iron to the ferric state.[10] The most widely accepted reaction mechanism for the hydroperoxidation is radical based, where the fatty acid is activated through oxidation by the ferric ion to form the fatty acid radical. This generates the ferrous/substrate radical intermediate which then is attacked regio- and stereospecifically by dioxygen to form only the S-configured product.[11] Klinman and co-workers have demonstrated that catalysis is fully rate limited by hydrogen abstraction above 32 °C, as seen by the temperature dependence of an unusually high kinetic isotope effect (KIE).[12] The large KIE (>60) is thought to be due to hydrogen atom tunneling, and the role of the metal may be significant in the process.[13]

† University of California, Santa Cruz.
‡ Stanford University.

(1) Gardner, H. W. *Biochim. Biophys. Acta* **1991**, *1084*, 221−239.
(2) Siedow, J. N. *Annu. Rev. Plant Physiol. Plant Mol. Biol* **1991**, *42*, 145−188.
(3) Ford-Hutchinson, A. W.; Gresser, M.; Young, R. N. *Annu. Rev. Biochem* **1994**, *63*, 383−417.
(4) Schewe, T.; Rapoport, S. M.; Kuehn, H. *Adv. Enzymol. Relat. Areas Mol. Biol* **1986**, *58*, 191−272.
(5) Yamamoto, S. *Biochim. Biophys. Acta* **1992**, *1128*, 117−131.
(6) Solomon, E. I.; Zhou, J.; Neese, F.; Pavel, E. G. *Chem. Biol.* **1997**, *4*, 795−808.
(7) Sigal, E. *Am. J. Physiol.* **1991**, *260*, L13-L28.
(8) Samuelsson, B.; Dahlen, S.-E.; Lindgren, J. A.; Rouzer, C. A.; Serhan, C. N. *Science* **1987**, *237*, 1171−1176.
(9) Gardner, H. W. *HortScience* **1995**, *30*, 197−205.
(10) DeGroot, J. J. M. C.; Veldink, G. A.; Vliegenhart, J. F. G.; Boldingh, J.; Wever, R.; Van Gelder, B. F. *Biochim. Biophys. Acta.* **1975**, *377*, 71−79.
(11) Gardner, H. W. *Biochim. Biophys. Acta* **1989**, *1001*, 274−281.
(12) Glickman, M. H.; Klinman, J. P. *Biochemistry* **1995**, *34*, 14077−14092.

10.1021/ja982844c CCC: $15.00
Published on Web 11/20/1998

Two X-ray crystal structures of the ferrous form of soybean lipoxygenase-1 (SLO-1) have been solved,[14,15] and both have identified two structural domains, a β-barrel and an α-helical region, the latter of which contains the active site iron. Both structures detect four common active site ligands, His_{499}, His_{504}, His_{690}, and the terminal carboxylate of Ile_{839}, each of these being conserved in all sequenced lipoxygenases (one exception is rat leukocyte 5-LO, which has a valine at the C terminus).[16] Boyington et al. have described the active site as four coordinate (4C) with two adjacent unoccupied ligand positions. Minor et al. have identified six ligands: the four ligands mentioned above, an additional water ligand, and a distant Asn_{694} (3.06 Å). The water points directly toward the mouth of the proposed substrate binding channel. EXAFS indicates that the bound water becomes a hydroxide upon oxidation of the iron and potentially is the base for substrate activation.[17]

Recently, a protocol using circular dichroism (CD) and magnetic circular dichroism (MCD) spectroscopies in the near-infrared (near-IR) spectral region in combination with ligand-field theory has been developed to explain the geometric and electronic structure of high-spin ferrous centers.[18] This protocol has addressed the structural differences between the two crystal structures described above. According to ligand-field theory and corresponding experimental studies on model complexes,[19] high-spin Fe^{2+} can exhibit at most two d → d transitions which occur in the near-IR spectral region. The energies of these two transitions will vary depending on the coordination environment of the iron. In general, 6C distorted octahedral ferrous sites show two transitions around 10 000 cm^{-1}, split by ~2000 cm^{-1}, while 5C sites show two transitions at ~10 000 and ~5000 cm^{-1}. Near-IR CD data of resting SLO-1 exhibit features at ~5000 and 10 700 cm^{-1} and a shoulder at ~8000 cm^{-1}.[20] The fact that there are three bands in the near-IR CD/MCD spectra of resting ferrous SLO-1 indicates that the site has a mixture of components in solution, and spectral simulations of these bands demonstrate that resting SLO-1 has a mixture of 5C and 6C species with an approximate 40:60% ratio, respectively. Addition of glycerol or substrate (anaerobically) shifts the 5C/6C mixture to a purely 6C form. This is a direct indication that there is coordination flexibility at the iron site. This flexibility is thought to be due to the Asn_{694} ligand, which varies in bond length between the crystal structures.

The importance of the Asn_{694} ligand in SLO-1 with respect to its spectroscopic data was tested by comparing the CD/MCD of the soybean enzyme with mammalian 15-LOs.[20] In comparing their sequences, it is predicted that the conserved Asn in plant LOs is a His in the mammalian 15-LOs (15-human LO (15-HLO) and 15-rabbit LO (15-RLO)), suggesting a dramatic iron coordination difference.[16] His is a stronger ligand than Asn, and an increased interaction with the iron would be expected. The low-temperature MCD spectra of the mammalian enzymes have d → d transitions around 8750 cm^{-1} with a shoulder around 10 700 cm^{-1}, consistent with a pure 6C ferrous site, indicating a His ligation to the metal.[20]

The His ligation is corroborated by the recent 15-RLO structure which has been solved with an inhibitor bound at the active site.[21] The iron coordination is similar to that of the soybean structure with three His's (2.1−2.3 Å) bound and a C-terminus carboxylate (2.1 Å); however, the Asn_{694} of SLO-1 has been replaced by a His_{545} in the rabbit structure (His_{544} in 15-HLO). The water ligand found in the soybean structure of Minor et al. is displaced in the rabbit structure by the inhibitor, whose carboxylate is directed toward the open coordination site of the iron atom (~4 Å).

The coordination effects of the change from an Asn to a His can also be observed in the ferric oxidation state using electron paramagnetic resonance (EPR) spectroscopy.[22] EPR spectroscopy detects the ground state which is classified by its degree of "rhombicity" as described by effective g values. Axial systems have effective g values of 6 and 2, while rhombic systems have effective g values around 4.3. From ligand-field theory, six ligands of comparable strength in the distorted protein environment provide a rhombic symmetry, while a very strong or weak ligand leads to an effective axial symmetry.[23] Thus, the EPR signal provides a direct probe of the ligand coordination environment. Wild-type (WT) SLO-1 displays an axial EPR signal,[24,25] which is surprising for non-heme enzymes. This can be explained by the weak Asn ligation in comparison to the other ligands which produces an axial effective symmetry around the iron (pseudo-5C). Mammalian LOs display rhombic EPR signals,[23] consistent with replacement of the Asn for a stronger His ligand. In summary, the mammalian 15-LOs are 6C in both the ferrous and ferric states with normal His ligation; however, the soybean enzyme is a mixture of 5C and 6C in the ferrous state (6C in the presence of the substrate) and pseudo-5C in the ferric state due to the weak Asn ligation.

This structural difference between the two enzymes at the sixth ligation site may have direct relevance to the rate-limiting hydrogen abstraction step by regulating the reactivity of the iron atom toward the substrate. Hydrogen abstraction may involve protonation of the bound hydroxide and reduction of the iron, both of which are effected by the strength of the ligands surrounding the iron. This hypothesis indicates the importance of the sixth ligand and reinforces the need to generate mutants at this site to determine its role in the catalytic mechanism. To date, one study has appeared pertaining to this question which contained preliminary EPR results on a different isozyme of soybean lipoxygenase, SLO-3.[26] In the current paper, we will describe the biochemical and physical properties of a mutant where the Asn in the soybean enzyme is converted to a His, which effectively converts it to the first coordination sphere of 15-HLO. This study includes near-IR CD/MCD measurements of the ferrous state and EPR spectroscopy of the ferric state, which provides information as to how perturbations at the sixth

(13) Jonsson, T.; Glickman, M. H.; Sun, S. J.; Klinman, J. P. *J. Am. Chem. Soc.* **1996**, *118*, 10319−10320.
(14) Boyington, J. C.; Gaffney, B. J.; Amzel, L. M. *Science* **1993**, *260*, 1482−1486.
(15) Minor, W.; Steczko, J.; Stec, B.; Otwinowski, Z.; Bolin, J. T.; Walter, R.; Axelrod, B. *Biochemistry* **1996**, *35*, 10687−10701.
(16) Sigal, E.; Craik, C. S.; Highland, E.; Grunberger, D.; Costello, L. L.; Dixon, R. A. F.; Jadel, J. A. *Biochem. Biophys. Res. Commun.* **1988**, *157*, 457−464.
(17) Scarrow, R. C.; Trimitsis, M. G.; Buck, C. P.; Grove, G. N.; Cowling, R. A.; Nelson, M. J. *Biochemistry* **1994**, *33*, 15023−15035.
(18) Solomon, E. I.; Pavel, E. G.; Loeb, K. E.; Campochiaro, C. *Coord. Chem. Rev.* **1995**, *144*, 369−460.
(19) Pavel, E. G.; Kitajima, N.; Solomon, E. I. *J. Am. Chem. Soc.* **1998**, *120*, 3949−3962.
(20) Pavlosky, M. A.; Zhang, Y.; Westre, T. E.; Gan, Q.-F.; Pavel, E. P.; Campochiaro, C.; Hedman, B.; Hodgson, K. O.; Solomon, E. I. *J. Am. Chem. Soc.* **1995**, *117*, 4316−4327.
(21) Gillmor, S. A.; Villasenor, A.; Fletterick, R.; Sigal, E.; Browner, M. *Nat. Struct. Biol.* **1997**, *4*, 1003−1009.
(22) Palmer, G. *Biochem. Soc. Trans.* **1985**, *13*, 548−560.
(23) Zhang, Y.; Gan, Q. F.; Pavel, E. G.; Sigal, E.; Solomon, E. I. *J. Am. Chem. Soc.* **1995**, *117*, 7422−7427.
(24) Gaffney, B. J. *Biophys. J.* **1993**, *64*, 773−783.
(25) Zhang, Y.; Gebhard, M. S.; Solomon, E. I. *J. Am. Chem. Soc.* **1991**, *113*, 5162−5175.
(26) Kramer, J. A.; Johnson, K. R.; Dunham, W. R.; Sands, R. H.; Funk, M. O. *Biochemistry* **1994**, *33*, 15017−15022.

site affect the coordination of the iron atom and how these changes pertain to the molecular mechanism.

Experimental Section

Source of Materials. Restriction endonucleases and polynucleotide kinase were obtained from New England BioLabs (Beverly, MA). 13-HPOD was HPLC purified from the reaction mixture of SLO-1 and linoleic acid, as previously described.[27] All other reagents were reagent grade or better and were used without further purification.

Plasmids and Strains. Plasmids for the mutagenesis (pL-1) and overproduction (pT-7/L-1) of SLO-1 were provided by Prof. Bernard Axelrod,[28] while plasmids for mutagenesis and overproduction (pSS15LO) of 15-HLO were provided by Dr. Elliott Sigal.[29] Site-directed mutagenesis was carried out by the Kunkel method. Uracil-containing single stranded (ss) DNA of pBluescript with SLO-1 (pL-1) and with 15-HLO (pSS15LO) were generated. The N694H SLO-1 sense strand primer (5′-CCATGCAGCCGTGCACTTTGGTCAGTATCC-3′) was annealed to SLO-1, while the H544N 15-HLO sense strand primer (5′-CGCCTCTGTGAACCTGGGCCAGC-3′) was annealed to 15-HLO. The double stranded (ds) DNA was synthesized with T4 DNA polymerase, ligated with T4 DNA ligase, and transformed into *Escherichia coli* XL1-Blue. Both genes were sequenced to verify the presence of only a single mutation. The mutated N694H SLO-1 gene was excised with BlpI and ClaI and ligated into pT-7/L-1 to place it under the control of the T7 promoter. This plasmid (pN694H) was transformed into *E. coli* BL21(DE3) for protein expression of N694H SLO-1. The mutated H544N 15-HLO gene from pSS15LO was linearized and cotransfected into recombinant baculovirus-infected *Spodoptera frugiperda* cells as described previously.[29]

Expression of Proteins. Cultures of *E. coli* BL21(DE3) were transformed with pT7-7 plasmids of SLO-1 genes. The cells were grown from single colonies in Luria−Bertani broth containing 100 μg/mL ampicillin. A 5-mL culture was incubated at 37 °C until cloudy and then serially diluted and grown to a final volume of 14 L. The cultures were shaken at 37 °C until absorbance at 600 nm attained 1.2 OD and then cooled to 15 °C with 3% ethanol added and grown overnight, as described previously.[28] The expression of H544N HLO in a baculovirus-insect cell culture system was performed as described previously.[29]

Purification of Proteins. The WT SLO-1 and mutant N694H SLO-1 were purified as follows. Induced cells were harvested by centrifugation and washed. The pellet was resuspended in 50 mL of 50 mM Tris-Base buffer (pH 7.5) containing 10% glycerol, 0.1% TritonX-100, and 500 mM NaCl. The cells were disrupted by three bursts of sonication (45 s) at 4 °C. Debris was removed by centrifugation at 27000*g* for 15 min and the pellet resonicated as above. The supernatants were combined and dialyzed for 2 h versus 20 mM Bis-Tris buffer (pH 6.0). The resulting supernatant was centrifuged at 27000*g* for 10 min and loaded directly onto a SP-Sephedex (Pharmacia) high-flow column (300 mL) which had been equilibrated with the same buffer. The column was washed with 5 column volumes of the buffer, and the enzyme was eluted with a step gradient of 500 mM NaCl and Bis-Tris (pH 6.0). Fractions containing lipoxygenase were pooled and dialyzed versus Bis-Tris (pH 6.0) overnight. The protein was then centrifuged (27000*g* for 10 min) and loaded onto a Bio-S 20 column (Bio-Rad). The column was washed with 5 volumes of the same buffer, and the enzyme was eluted with a 400-mL linear gradient from 0 to 500 mM NaCl and Bis-Tris (pH 6.0). The fractions with enzyme were pooled (≈200 mM NaCl), diluted 2-fold to 100 mM borate (pH 9.2), and concentrated in an Amicon pressure concentrator to a minimal volume (membrane YM-30). WT SLO-1 and N694H SLO-1 were routinely obtained with a final yield of ≈5 mg/L of cells. The purity of the enzyme was greater than 95% as seen by SDS-PAGE. The wild-type 15-HLO and H544N 15-HLO were purified as described previously with no modifications.[29]

Enzyme activity was determined by monitoring the absorption of the product formed during the enzymatic reaction at 234 nm ($\epsilon_{234} = 2.5 \times 10^4$ M^{-1} cm^{-1}). The iron contents of all lipoxygenases were determined by a Finnegan ICP-MS, using standardized iron solutions. Ferric enzymes were generated by the addition of a stoichiometric amount of the peroxide product, 13-HPOD, to the native ferrous enzyme.

Near-IR CD and MCD Spectroscopies were performed on a Jasco J200D spectropolarimeter (600−2100 nm) with liquid N_2-cooled InSb detector. N694H SLO-1 CD samples (∼2 mM) were buffered in 50 mM deuterated CHES (pD = 9.0), and the spectra were obtained using a 1-cm path length cell, kept at 5 °C. CD spectra are baseline corrected for the buffer and cell background. MCD samples contain 55% (v/v) glycerol-d_3 as a low-temperature glassing agent. (Note: no change in CD after addition of glycerol.) The MCD spectra were obtained from 0.3-cm-thick glass samples sandwiched between two Infrasil quartz disks in a MCD cell, which is securely placed in a variable-temperature insert in an Oxford Instruments SM4000-7T superconducting magnet, capable of fields up to 7 T and temperatures down to 1.5 K. Depolarization of frozen MCD samples was judged to be <5% by comparing the CD spectra of a nickel (+)-tartrate solution placed before and after the sample. MCD spectra were corrected for the natural CD and zero-field baseline effects due to the optical quality of the frozen sample by subtracting the corresponding 0 T scan at each temperature.

EPR Spectroscopy. EPR measurements were performed on a Bruker ESP 320 spectrometer fitted with a dielectric resonator and companion helium cryostat. The temperature was measured continuously using a cernox sensor (Lakeshore Cryotronics) placed directly above the sample, in a 4-mm-o.d. quartz tube. Data manipulation and EPR spectral simulations were performed using the program HAM, provided by Dr. M. Hendrich. The signals were fit with an effective $S = {}^1/_2$ model which uses a *g*-dependent line width tensor and properly accounts for field-dependent transition probabilities. The temperature dependence was also fit with this program using standard Boltzmann equations. The amount of EPR-active Fe^{3+} in the protein samples was determined relative to an Fe^{3+} EDTA standard. This standard was made with iron from an atomic absorption standard of known concentration and addition of 10-fold excess of EDTA in a 50% solution of glycerol. The EPR spectra were measured at 4.3 K and a microwave power of 31 μW, which was determined to be well below the level of power saturation.

UV/Vis CD Spectroscopy was obtained at 10 °C using an Aviv 60DS spectrophotometer. CD spectra are baseline corrected by subtracting the buffer and cell backgrounds from the raw data. Titrations were performed by the addition of 1 equiv of 13-HPOD (evaporated) to 0.6 mL of lipoxygenase (20 mg/mL).

Results and Analysis

Mutagenesis, Expression, and Purification. N694H SLO-1 was expressed using pN694H in *E. coli* (∼5 mg/L),[28] and H544N 15-HLO was expressed from a baculovirus-insect cell culture system (∼20 mg/L).[29] Both mutants were purified as previously described to >90% purity as judged by SDS-PAGE, stained with Commassie brilliant blue (data not shown).

Kinetic Analysis of N694H Soybean Lipoxygenase-1. As isolated, ICP-MS indicates that N694H SLO-1 contains 0.55 ± 0.1 mol of iron per mol of enzyme. The N694H mutant retains the same regio- and stereospecificity of product formation as the WT enzyme and converts linoleic acid to the 13-(*S*)-HPOD product, as seen by chiral column analysis.[30] N694H SLO-1 exhibits a pronounced kinetic lag phase which can be eliminated with addition of a large excess of product (∼1000 equiv). This is in contrast to WT SLO-1, which exhibits a smaller lag phase and has a markedly lower requirement of 13-HPOD for activation (<5 equiv). The calculated k_{cat} and K_m from initial rate determinations are 10 ± 2 s^{-1} and 4 ± 1 μM, respectively (corrected for 55% percent iron content), which

(27) Nelson, M. J.; Cowling, R. A.; Seitz, S. P. *Biochemistry* **1990**, *29*, 6897−6903.

(28) Steczko, J.; Donoho, G. A.; Dixon, J. E.; Sugimoto, T.; Axelrod, B. *Prot. Exp. Pur.* **1991**, *2*, 221−227.

(29) Sloane, D. L.; Leung, R.; Barnett, J.; Craik, C. S.; Sigal, E. *Prot. Eng.* **1995**, *8*, 275−282.

(30) Courtesy of Prof. Bernard Axelrod.

Table 1. Experimental Enzyme Kinetic Parameters[a]

	k_{cat} (s^{-1})	K_m (μM)	k_{cat}/K_m ($s^{-1}\,\mu M^{-1}$)	$(k_{cat}/K_m)^H/(k_{cat}/K_m)^D$	K_i (μM oleic acid)
N694H SLO-1	10 ± 2	4 ± 1	2.5 ± 1.1	60 ± 9	8 ± 1
WT SLO-1[12]	280 ± 8	11 ± 2	25 ± 5	48 ± 5	22 ± 2[32]
WT 15-HLO[31]	6.2 ± 0.1	7.8 ± 0.5	0.79 ± 0.06	59 ± 6	nd[b]

[a] The temperature for all kinetic experiments was 25 °C, except for the KIE experiments which were performed at 30 °C, using a novel RP-HPLC competitive method.[37] [b] nd = not determined.

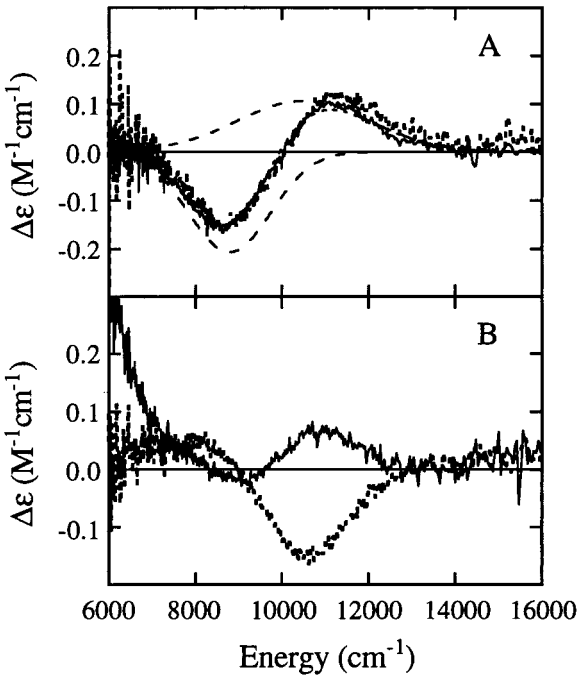

Figure 1. Near-IR circular dichroism spectra at 4 °C of (A) resting N694H SLO-1 in 50 mM CHES, pD 9.0 (light solid line) with Gaussian components (light dashed lines) and Gaussian sum (light dotted line), and resting N694H SLO-1 in 50 mM CHES, pD 9.0 + 50% (v/v) glycerol-d_3 (dark dotted line) and (B) resting WT SLO-1 in 50 mM CHES, pD 9.0 (light solid line), and resting WT SLO-1 in 50 mM CHES, pD 9.0 + 50% (v/v) glycerol-d_3 (dark dotted line). Adapted from ref 20.

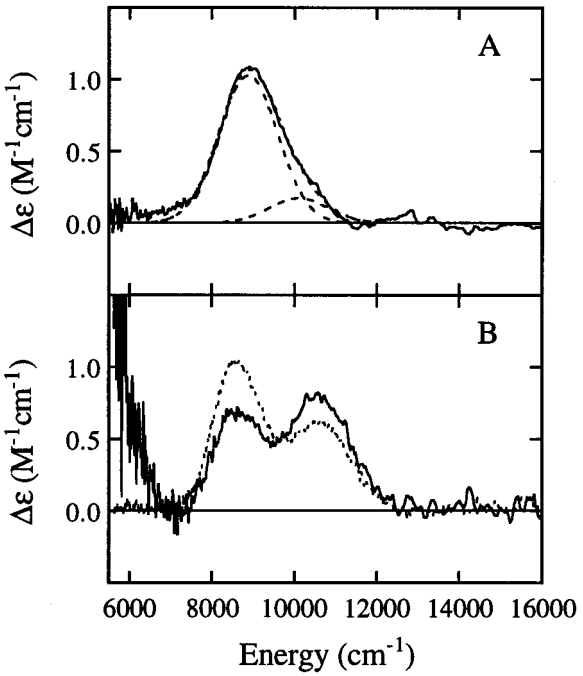

Figure 2. (A) Near-IR magnetic circular dichroism spectra at 7 T and 5.0 K of resting N694H SLO-1 in 50 mM CHES, pD 9.0 + 50% (v/v) glycerol-d_3 (light solid line) with Gaussian components (light dashed lines) and Gaussian sum (light dotted line). (B) Near-IR magnetic circular dichroism spectra at 6 T and 4.2 K of resting WT SLO-1 in 50 mM CHES, pD 9.0 saturated with sucrose (light solid line), and resting WT SLO-1 in 50 mM CHES, pD 9.0 + 50% (v/v) glycerol-d_3 (dark dotted line). Adapted from ref 20.

are different from those for both WT SLO (280 ± 8 s^{-1} and 11 ± 2 μM)[12] and WT 15-HLO (6.2 ± 0.1 s^{-1} and 7.8 ± 0.5 μM)[31] (Table 1). Oleic acid, a competitive inhibitor of WT SLO-1, also inhibits the N694H mutant with a K_i of 8 ± 1 μM, which is less than that for WT SLO (22 ± 2 μM).[32] These results are summarized in Table 1**.**

Kinetic Analysis of H544N Human 15-Lipoxygenase. As isolated, H544N 15-HLO exhibits no activity because the critical iron atom is not bound in appreciable amounts (<1% iron from ICP-MS). Attempts to insert metal into the mutant through dialysis were unsuccessful.

Near-IR CD/MCD of N694H SLO-1: Comparison to WT SLO-1 and 15-RLO. CD and MCD in the near-IR region allow one to directly observe the energy splitting of the e_g set of 3d orbitals of the high-spin Fe^{2+} site. This splitting is sensitive to the ligand field imposed by the protein ligands and can be correlated to coordination number and geometry at the Fe^{2+} site.[18] The near-IR CD spectrum of resting N694H SLO-1 (Figure 1A, light solid line) shows one negative peak at ~9000 cm^{-1} and one positive peak at ~11 000 cm^{-1}. Addition of glycerol to resting N694H SLO-1 does not affect the CD spectrum (Figure 1A, dark dotted line). Gaussian fitting of the resting N694H SLO-1 CD spectrum gives a negative band at 9050 cm^{-1} and a positive band at 10 400 cm^{-1}. This shows that resting N694H SLO-1 has a 6C ferrous active site with distorted octahedral geometry and glycerol does not perturb the active site. This is in contrast to the previously reported near-IR CD spectrum of resting WT SLO-1 (Figure 1B, light solid line), which is a 40%/60% mixture of 5C and 6C species that converts to a pure 6C species upon binding glycerol, other alcohols, or substrate (Figure 1B, dark dotted line).[20] Alternatively, as reported previously,[20] 15-RLO exhibits two bands at ~8500 and 10 500 cm^{-1}, which indicates a 6C species regardless of solvent conditions.

The 5 K, 7 T MCD spectrum of resting N694H SLO-1 in glycerol is presented in Figure 2A and contains a broad unsymmetric feature at ~10 000 cm^{-1}. This feature can be Gaussian resolved into two bands at 9050 and 10 400 cm^{-1} (Figure 2A, light dashed lines) to give $\Delta^5E_g = 1350$ cm^{-1} (see Table 2), indicating again a pure distorted octahedral 6C ferrous active site in resting N694H SLO-1. For comparison, the previously reported low-temperature MCD spectra of resting WT SLO-1 in saturated sucrose[20] (a nonperturbing low-temperature glassing agent) and glycerol are also shown in Figure 2B (light solid line and light dotted line, respectively),

(31) Gan, Q.-F.; Browner, M. F.; Sloane, D. L.; Sigal, E. *J. Biol. Chem.* **1996**, *271*, 25412−25418.

(32) Van der heijdt, L. M.; Schilstra, M. J.; Feiters, M. C.; Nolting, H. F.; Hermes, C.; Veldink, G. A.; Vliegenthart, J. F. G. *Eur. J. Biochem.* **1995**, *231*, 186−191.

Table 2. Experimental d-Orbital Splittings and Ligand-Field Parameters

parameters	N694H SLO-1 (9090 cm^{-1})	6C SLO-1[a] (8600 cm^{-1})	15-RLO[a] (8600 cm^{-1})
Δ^5E_g (cm^{-1})	1350	1700	1650
$g_{\|\|}$	10.3	10.5	9.0
δ (cm^{-1})	9.6	9.6	4.4
Δ (cm^{-1})	$+400 \pm 200$	$+450 \pm 200$	-500 ± 200
$\|V\|$ (cm^{-1})	150 ± 100	150 ± 110	270 ± 160
$\|V/2\Delta\|$	0.18 ± 0.05	0.16 ± 0.05	0.27 ± 0.05

[a] Data for 6C SLO-1 and 15-RLO are from ref 20.

indicating that the resting WT SLO-1 is a mixture of 5C and 6C species in sucrose (a nonperturbing glassing agent) and is converted to a pure 6C species in glycerol. In contrast to WT SLO, WT 15-RLO shows an MCD spectrum with two bands at 8650 and 13 300 cm^{-1}, consistent with a 6C species which is not perturbed by solvent.[20]

Near-IR VTVH MCD of N694H SLO-1: Comparison to WT SLO-1 and 15-RLO. While the excited-state CD and MCD data are related to the energy splitting of the e_g set of the 3d orbitals of high-spin Fe^{2+} site, the VTVH MCD data provide further information about the splittings of the t_{2g} set. [18] The high-spin d^6 electron configuration of Fe^{2+} gives rise to a total spin of $S = 2$ with five spin components $M_S = 0, \pm1, \pm2$. In low-symmetry environments, the 5-fold spin degeneracy is completely lifted even in the absence of an external magnetic field (i.e., zero-field splitting (ZFS)). For negative ZFS systems ($D < 0$), the non-Kramers doublet $M_S = \pm2$ is lowest in energy and split by the rhombic ZFS (δ). For +ZFS systems ($D > 0$), the lowest component is the $M_S = 0$ singlet, which, together with one component of the $M_S = \pm1$ first excited doublet at an energy D, forms a pseudodoublet ground state. +ZFS systems can be distinguished from −ZFS by a large sublevel splitting ($\sim D$ instead of δ). The observed MCD intensity comes from the population difference of the sublevels at low temperature. VTVH MCD data consist of MCD intensities collected over a range of temperatures and magnetic fields at a fixed wavelength and are usually presented in a plot of MCD intensity versus $\beta H/2kT$ (where β is the Bohr magneton and k is Boltzmann constant). The larger the ground-state splitting, the more spread the isotherms will be in a $\beta H/2kT$ plot. Fitting the experimental VTVH MCD to theoretical expressions allows the estimation of δ (or D) and g. These ground-state spin Hamiltonian parameters can then be directly related to the splittings of the t_{2g} orbital set, where Δ is defined as $E_{d_{xz},d_{yz}} - E_{d_{xy}}$ and V is $|E_{d_{xz}} - E_{d_{yz}}|$. [18]

Figure 3A shows VTVH MCD data (symbols) for N694H SLO-1 taken at 9050 cm^{-1} and the best theoretical fit (lines). The saturation magnetization curves for different temperatures are not superimposable and indicate an integer spin $S = 2$ ground state.[20] The large nesting of the saturation magnetization data yields $\delta = 9.6$ cm^{-1} and $g = 10.3$, corresponding to $D = +14$ cm^{-1} and $|E/D| = 0.1$. The ground-state parameters could be related to the t_{2g} orbital splittings and yields $\Delta = +400 \pm 200$ cm^{-1} and $|V| = 150 \pm 100$ cm^{-1}. This t_{2g} splitting is indicated as in the inset in Figure 3A.

The nesting behavior of the VTVH MCD of resting N694H SLO-1 and its best-fit parameters (see Table 2) are strikingly similar to those reported[20] for the 6C species of WT SLO-1, which are shown in Figure 3B for comparison. They have the same δ and g values, which correlates to the same positive D and $|E/D|$ values and, thus, the same t_{2g} orbital splittings (Table 2 and insets in Figure 3A,B). Also shown for comparison is the previously reported VTVH MCD data and fit for ferrous 15-RLO (Figure 3C),[20] which shows a much smaller nesting of the isotherms. The fit of the 15-RLO VTVH MCD data resulted in a smaller δ value, indicating a $-D$ system and a different t_{2g} splitting pattern (inset in Figure 3C and Table 2) from those of WT and N694H SLO-1.

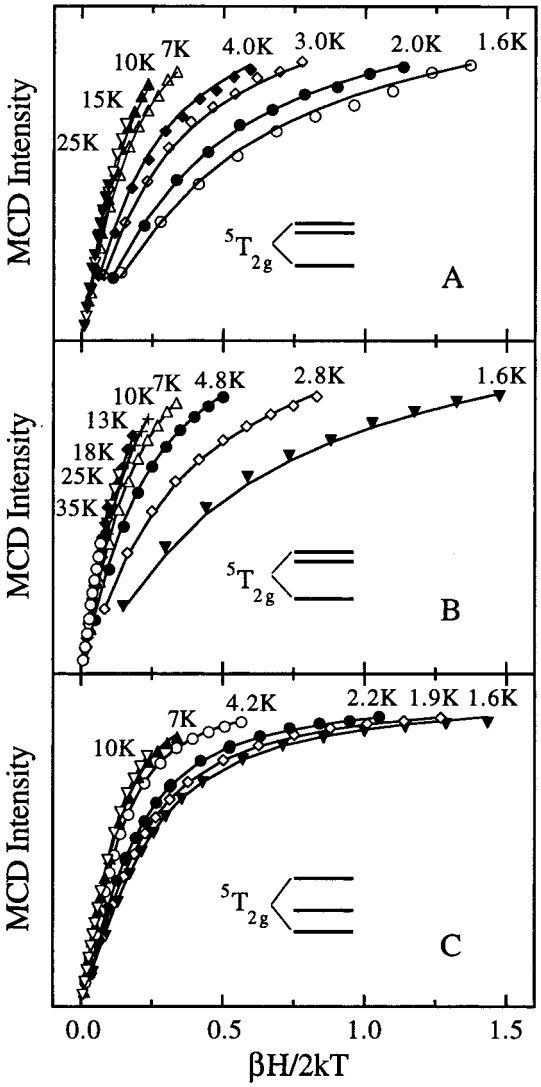

Figure 3. Saturation magnetization curves of the MCD intensity plotted as a function of $\beta H/2kT$ for (A) resting N694H SLO-1 obtained for the 9090 cm^{-1} band in Figure 2A, (B) resting SLO-1 obtained for the 8600 cm^{-1} band in Figure 2B (adapted from ref 20), and (C) resting 15-RLO for the 8600 cm^{-1} band in Figure 5B in ref 20. The insets describes the different t_{2g} orbital splittings for the corresponding species.

EPR Spectra of Resting and Oxidized N694H Soybean Lipoxygenase. The EPR spectrum of N694H SLO-1 (0.55 Fe/enzyme) in frozen solution at 4.3 K exhibits a weak signal at $g \approx 4.3$ (data not shown). The low-intensity signal at $g \approx 4.3$ represents less than $\approx 0.5\%$ of the total iron as determined by spin quantitation (vide infra). This indicates that the mutant, as isolated, is in the reduced ferrous form. Addition of 10 equiv of 13-(*S*)-HPOD to ferrous N694H SLO-1 oxidizes the iron to the catalytically competent ferric species. The ferric form of N694H SLO-1 demonstrates a complex multicomponent EPR signal with pronounced features around $g \approx 4.3$, 6, and 7.7 (Figure 4A). The signals with g values of 6 and 7.7 are anisotropic and spread over a wide field range (approximately 2300 G). Any features with g values around 2 are obscured by an adventitious Mn^{2+} signal.

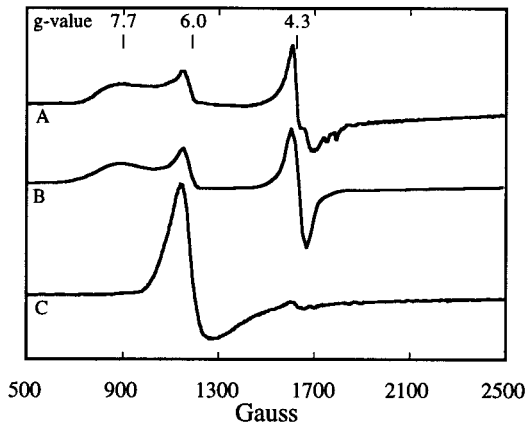

Figure 4. (A) Low-temperature (4.3 K) EPR spectrum of oxidized N694H SLO-1 (210 μM Fe^{3+}) in 100 mM borate and 0.2 M NaCl (pH 9.2). (B) Simulation of oxidized N694H SLO-1 (75 ± 15% intermediate rhombicity, 16 ± 5% axial, and 9 ± 5% rhombic). (C) Low-temperature (4.3 K) EPR spectrum of oxidized WT SLO (110 μM Fe^{3+}, normalized to N694H SLO-1 Fe^{3+} concentration, 210 μM) in 100 mM borate and 0.2 M NaCl (pH 9.2). Spectrometer settings: field set = 2050 G, scan range = 4000 G, time constant = 82 s, mod. amplitude = 20 G, microwave power = 31 μW, frequency = 9.71 GHz, gain = 1000.

EPR spectra are classified phenomenologically by their ligand-field symmetries and can range from rhombic to axial.[22] The classification of spectra into axial and rhombic forms can be put on a more quantitative basis using the ZFS parameters D and E/D. D describes the axial zero-field splitting of the $S = {}^5/_2$ electronic ground state ($M_S = \pm{}^1/_2$ at 0, $\pm{}^3/_2$ at $2D$, and $\pm{}^5/_2$ at $4D$ for positive ZFS). E/D defines the rhombicity of the ligand field. By definition, E/D can only vary from 0 (axial) to 0.33 (rhombic). High-spin, ferric iron sites with axial symmetry ($E/D = 0$) exhibit a spin transition within the $\pm{}^1/_2$ doublet which produces an anisotropic signal with features at $g = 6$ and $g = 2$. As the symmetry becomes more rhombic, the spectra shifts to $g \approx 4.3$ ($E/D = 0.33$). This rhombic signal arises from transitions within the first excited doublet of the rhombic $S = {}^5/_2$ manifold (at an energy $Z = 3.4D$ above the ground sublevel). The EPR intensity of the 4.3 signal is very strong since all three g values are similar and can be a prominent feature in the spectra even at low concentration.[22]

In analyzing the spectrum of the N694H mutant in Figure 4A, the $g \approx 6$ signal has axial symmetry ($E/D = 0$) with g values of 6 and 2, while the signal at 7.7 is ascribed to a site with intermediate rhombicity with an E/D of 0.08. The feature at $g = 4.3$ is due to a rhombic species. These features indicate that the oxidized mutant contains no less than three species: axial ($g_{x,y,z} = 6, 6, 2$), intermediate rhombicity ($g_{x,y,z} = 7.7, 4.1, 1.8$), and rhombic ($g_{x,y,z} = 4.3, 4.3, 4.3$).

Simulation, Temperature Dependence, and Quantification of the Iron EPR Signals. The quantification of the amount of Fe^{3+} contributing to the axial ($g \approx 6$), intermediate rhombicity ($g \approx 7.7$), and rhombic ($g \approx 4.3$) signals is complicated by the fact that the axial and intermediate rhombicity signals are spread over a large field range (≈2300 G) and overlap. This problem can be overcome by EPR simulations. The simulated spectra are simultaneously integrated over the entire field range to obtain the total EPR intensity from transitions within the $M_S = \pm{}^1/_2$ Kramers doublet for the axial and intermediate rhombicity signals and the middle transition of the rhombic signal. Fe^{3+}-(EDTA) was used as a standard for spin quantitation. The double integral was evaluated between 0 and 2500 G, just short of the interfering signal from adventitious Mn^{2+}. The signals for the oxidized N694H SLO-1 were simulated with an effective spin $S' = {}^1/_2$ Hamiltonian (Figure 4B), with the parameters given in Table 3. An axial doublet ($g \approx 6$), a doublet with intermediate rhombicity ($g \approx 7.7$), and two rhombic doublets ($g \approx 4.3$) were required for simulation. The two rhombic doublets were required because one would not adequately fit the broad base of the $g \approx 4.3$ signal. These two rhombic components are considered as a single species in the following discussion. The simulation areas were adjusted for the g_{av} differences of the rhombic and axial signals as described by Assa and Vanguard,[33] and line width broadening was applied to each g value.

Table 3. Theoretical EPR Simulation Parameters

	E/D	$g_x(\Delta g)^a$	$g_y(\Delta g)^a$	$g_z(\Delta g)^a$
sim 1, axial 1	0.0	6.0 (19)	6.0 (155)	2.0 (170)
sim 2, intermed. rhombic	0.08	7.7 (93)	4.1 (333)	1.8 (170)
sim 3, rhombic 1	0.33	4.3 (114)	4.3 (114)	4.3 (114)
sim 4, rhombic 2	0.33	4.5 (34)	4.3 (23)	4.0 (43)

[a] Line widths in gauss (G) at half-height of the absorption curve are given in parentheses.

Quantification of the signal intensity is dependent on the relative populations of the spin manifolds of each for the three EPR active species. To account for the spin populations of all the three M_S doublets, the ZFS parameters were determined for each species from the temperature dependence of the EPR spectral intensity over the range 1.8−55 K. The temperature dependence of the $g \approx 7.7$ and $g \approx 4.3$ signals were evaluated, and their signal intensity versus temperature (Figure 5) were fit to the Boltzmann equation by nonlinear regression, with the proportionality constant K and zero-field splitting constant D as adjustable parameters. For the intermediate rhombicity species ($g \approx 7.7$) (Figure 5A), the ZFS was determined to have a positive D with a value of 2 ± 1 cm^{-1}, while the rhombic $g \approx 4.3$ signal (Figure 5B) had an energy difference between doublets ($Z = 3.5D$) of 3.5 ± 0.8 cm^{-1}, giving a $|D|$ of 1 ± 0.2 cm^{-1}. These ZFS parameters were used to calculate the Boltzmann population distributions of the three doublets, and the spin populations were corrected accordingly for the two signals, $g \approx 4.3$ and $g \approx 7.7$. The $g \approx 6$ signal had significant spectral overlap with the other two species, and therefore, its temperature dependence could not be obtained accurately from the EPR spectral data. Its D value was set to 2 cm^{-1}, based on the results for the intermediate rhombicity signal and the fact that, in WT SLO-1, two axial signals are observed with D values of approximately 2 cm^{-1}.[34]

Utilizing both the intensity simulation (g_{av} corrected) and the Boltzmann population factors, it was determined that the concentrations of the three EPR visible species account for approximately 56 ± 10% of the total iron content (380 μM measured by ICP-MS and 213 μM by simulation). The proportionality of the three species in the oxidized N694H mutant is 16 ± 5% axial, 75 ± 15% intermediate rhombicity, and 9 ± 5% rhombic. It is important to note the dominant species present in the N694H mutant is the intermediate rhombicity signal ($E/D = 0.08$) at $g_{eff} = 7.7$, while the dominant species in the WT SLO-1 (97%) is the axial ($E/D = 0.01$) species at $g_{eff} \sim 6$ in Figure 4C.

Chemical Perturbations. As mentioned previously, the N694H mutant requires 10-fold excess of product to oxidize the EPR signal completely. Addition of 30-fold excess does not produce a purple species associated with hydroperoxide

(33) Aasa, R.; Vanngard, T. *J. Magn. Res.* **1975**, *19*, 308−315.
(34) Slappendel, S.; Veldink, G. A.; Vliegenhardt, J. F. G.; Aasa, R.; Malmström, B. G. *Biochim. Biophys. Acta* **1980**, *642*, 30−39.

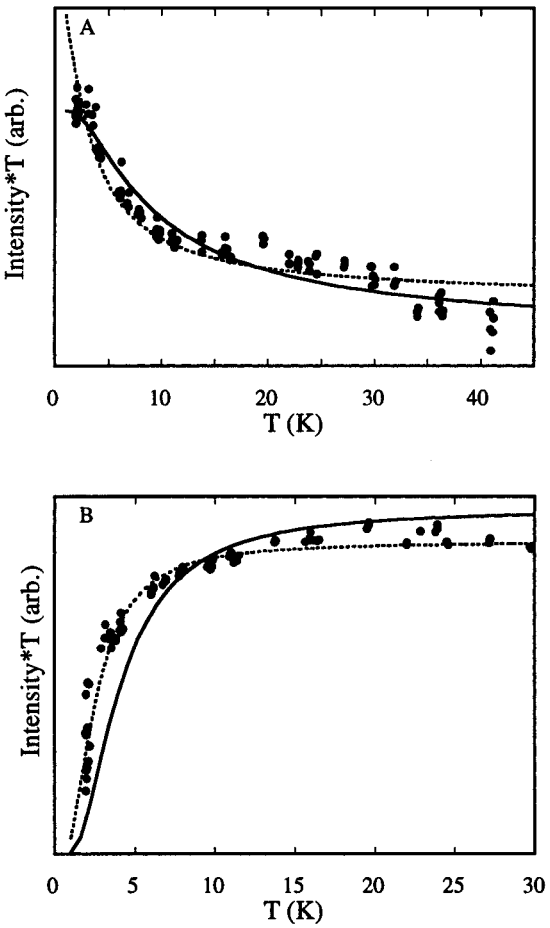

Figure 5. (A) Temperature dependence of the EPR signal intensity of oxidized N694H SLO-1, as measured by the amplitude changes of the signal at $g \approx 7.7$. Fits obtained for the population of three doublets separated by $D = 1$ cm^{-1} (dashed line) and $D = 3$ cm^{-1} (solid line). (B) Temperature dependence of the EPR signal intensity of oxidized N694H SLO-1, as measured by the amplitude changes of the signal at $g \approx 4.3$. Fits obtained for population of three doublets equally separated by 2.8 cm^{-1} (dashed line) and 4.2 cm^{-1} (solid line). The EPR parameters for both temperature studies are the same as in Figure 4.

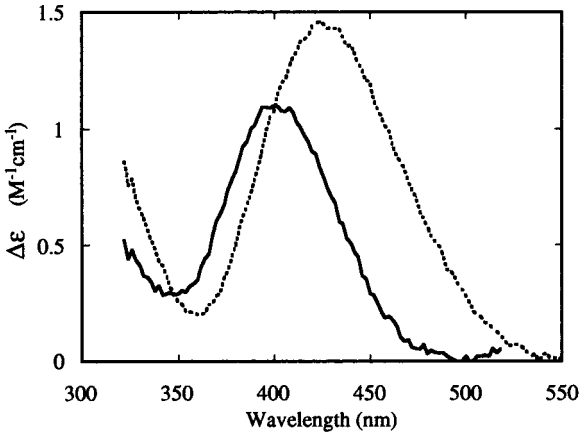

Figure 6. CD Spectra of oxidized WT SLO-1 (210 μM) (dashed line) and oxidized N694H SLO-1 (210 μM) (solid line) taken at 10 °C. Samples were corrected for metal content.

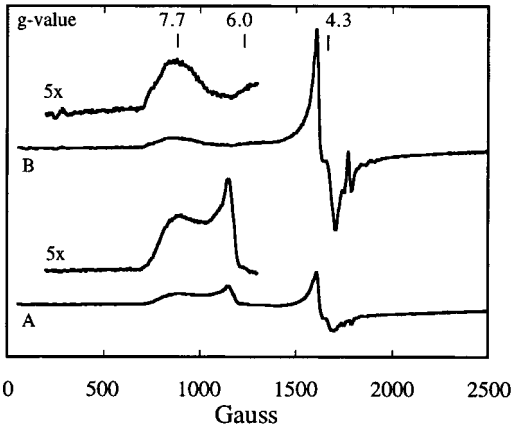

Figure 7. Low-temperature (4.3 K) EPR spectra of (A) N694H SLO-1 (210 μM Fe^{3+}) oxidized with 10 equiv of 13-HPOD, (B) oxidized N694H SLO-1 sample (210 μM Fe^{3+}) in 100 mM borate buffer, 0.2 M NaCl (pH 9.2), and 0.1% ethanol. Spectrometer settings: field set = 2050 G, scan range = 4000 G, time constant = 82 s, mod. amplitude = 20 G, microwave power = 31 μW, frequency = 9.71 GHz, gain = 1000. Features around 1800 G are artifacts due to cavity signal subtraction.

product binding. This is in contrast to the WT enzymes from soybean and rabbit which only require 1 equiv to fully oxidize the enzyme and 3 equiv to produce the purple species.[27] The lack of a visible purple species for the mutant is similar to the behavior of 5-HLO, which can be oxidized by product but does not convert to a purple species with excess product.[35] The oxidation of the mutant is accompanied by an increase in absorbance intensity at 350 nm (the yellow species, i.e., Fe^{3+} form). This is assigned as a His$-$Fe^{3+} ligand-to-metal charge-transfer (LMCT) transition as observed for other lipoxygenases.[25] UV$-$vis CD spectroscopy resolves the LMCT band from the large protein envelope, and the spectra of both SLO-1 and N694H SLO-1 display well-isolated bands with distinct maxima (Figure 6). The WT band has a maximum of 425 nm (23 800 cm^{-1}), while the N694H band is shifted to 400 nm (25 000 cm^{-1}). These maxima are unaffected by glycerol and concentration variations. The $\Delta\epsilon$ values for WT and N694H SLO-1 have been corrected for iron content and are of comparable magnitude ($\Delta\epsilon = 1.5$ and 1.1 M^{-1} cm^{-1}, respectively).

Addition of ethanol (1%) or glycerol (40%) affects the EPR signal of N694H SLO-1 by shifting the relative proportions of the three major species. There is a small increase in the rhombic species (from 9% to 20%) with a concomitant decrease in the axial species (from 15% to 0%) (Figure 7A, B). This increase in the rhombic species is reversible through dialysis, indicating a structural perturbation rather than a loss of the iron due to denaturation. There is no change in the amount of intermediate rhombicity signal which is still the dominant species present (70 $\pm$ 15%) in the purturbed systems. Variations of buffers (Tris, Bis-Tris, HEPES, and CHES) and pH (from 6 to 11) and addition of inhibitors (oleic acid) do not significantly effect the EPR signal. This is in contrast to the observed dependence of the WT SLO-1 spectrum upon buffer and pH change.[24,36]

Discussion

The ferrous form of the N694H SLO-1 displays a near-IR CD spectrum typical of a 6C ferrous species which is not affected by glycerol. This is in contrast to the WT SLO-1, which exists as a mixture of 5C and 6C ferrous species (40:60,

(35) Chasteen, N. D.; Grady, J. K.; Skorey, K. I.; Neden, K. J.; Riendeau, D.; Percival, M. D. *Biochemistry* **1993**, *32*, 9763−9771.

(36) The N694H mutant was purified after oxidation to remove excess product, and no signal change was noted. However, over the 2-h purification process, approximately 60% of the signal intensity was lost. The WT SLO-1, under the same purification conditions, did not lose appreciable intensity.

respectively) and is converted to pure 6C upon addition of glycerol, alcohols, or substrate.[20] The VTVH MCD data for N694H SLO-1 ($\Delta \approx +400$ cm^{-1}), however, are remarkably similar to those for the 6C component of the WT SLO-1, despite the coordination change from Asn to His.[20] The CD/MCD spectra of 15-HLO and 15-RLO exhibit a 6C Fe^{2+} site,[20] similar to that of the N694H mutant, but the VTVH dependence of the MCD spectra is markedly different than those of N694H and 6C−WT SLO-1, with respect to ground-state parameters ($\Delta \approx -500$ cm^{-1}). This indicates that the splitting of the t_{2g} orbitals has the opposite sign relative to 6C WT SLO-1 and N694H SLO-1.[20] The ferric EPR signal of N694H SLO-1 is predominately of intermediate rhombicity with an E/D value of ≈0.08, which is between the axial WT SLO-1 ferric signal ($E/D \approx 0.01$, pseudo-5C)[24] and the rhombic WT 15-HLO ($E/D \approx 0.33$, 6C).[23] The EPR signal also contains a small percentage of rhombic iron which is increased upon addition of glycerol or ethanol, indicating some heterogeneity and flexibility of the coordination environment. Both the ferrous CD/MCD and ferric EPR data indicate that the coordination geometry and electronic structure of the iron site of the N694H mutant are between those of the WT soybean and mammalian enzymes. This is due to the fact that the His is a stronger ligand than Asn, which produces a pure 6C ferrous iron as seen by CD/MCD. However, the His in N694H SLO-1 is a weaker ligand than that in the WT mammalian enzymes, as seen by the positive t_{2g} splitting in the ferrous MCD (Δ in Table 2) and an intermediate rhombicity signal in the ferric EPR (Table 3). This indicates that the His is not in its most favorable conformation for binding to the iron atom in SLO-1, likely due to its evolutionary optimization for Asn.

While WT SLO-1 and 15-HLO are structurally very similar,[21] their sequence homology is only 25%, which may affect substrate binding. However, the K_m for N694H SLO-1 is similar to both WT SLO-1 and 15-HLO, indicating that there are only minor changes in the substrate binding cavity between the three enzymes. It is important to note that the small reduction in K_m for 15-HLO and N694H SLO-1 relative to WT SLO-1 (Table 1) is not due to a change in their dissociation constants (K_D) but rather to their reduced k_{cat} values. As previously defined by Glickman et al., the K_m ($=(k_{-1} + k_{cat})/k_1$) is not the K_D ($=k_{-1}/k_1$), except when k_{cat} is much smaller than k_{-1}. 15-HLO and N694H SLO-1 appear to be close to this limit. The k_{cat} difference between WT SLO-1 (280 ± 8 s^{-1})[12] and 15-HLO (6 ± 0.1 s^{-1})[29] could be complicated by the significant sequence differences. However, the fact that k_{cat} for N694H SLO-1 fits between those for the plant and mammalian WT enzymes strongly suggests that the first coordination sphere change correlates with the kinetic change. This kinetic change is likely due to a decrease in the hydrogen atom abstraction efficiency and not other possible contributing factors (i.e., viscosity and H-bond rearrangement[12]); all three enzymes manifest a similar, large KIE ($=(k_{cat}/K_m)^H/(k_{cat}/K_m)^D$) (Table 1) under conditions (30 °C) where hydrogen atom abstraction is the rate-limiting factor.[37]

The generally accepted molecular mechanism for lipoxygenase is shown in Scheme 1, where the ferric hydroxide species (I) abstracts a hydrogen atom from linoleic acid, generating the ferrous water species (II) and the substrate radical which subsequently reacts with oxygen to form the hydroperoxide product. As shown by Mayer and co-workers,[38] the driving force of the hydrogen atom abstraction is related to the strength

Scheme 1

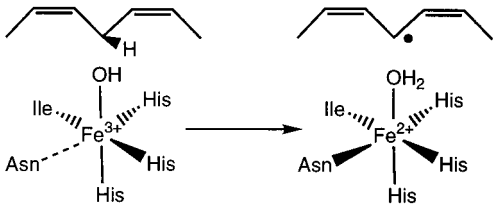

I **II**

of the OH bond produced in the abstraction intermediate (species II), which through a Born scheme is related to the reduction potential ($E°$) of the Fe^{3+}/Fe^{2+} couple and the pK_a of the abstracted proton in the ferrous species II. A high reduction potential and a high pK_a of the bound water in the reduced species II increases the hydrogen atom abstraction driving force and thus the catalytic rate. The structural changes we observe in the spectroscopies of the three enzymes can strongly affect the reduction potentials and the pK_a's of the reduced species II and hence catalysis (i.e., k_{cat}). Increasing the donor ability of the varied ligand to the iron will reduce its effective nuclear charge and thus its inductive effect on the coordinated water in species II and hence raise the pK_a. MCD studies show that the reduced ferrous site in WT SLO-1 shows no change up to pH 11 (Supporting Information). An ∼20% change in the spectrum would have been easily observed. This places a lower limit of the pK_a of the coordinated water in the ferrous species II of 11.5 in WT SLO-1. For N694H SLO-1 and 15-HLO, replacement of the Asn with the stronger His ligand, which is a better donor to the metal, should raise the pK_a of the coordinated water of the ferrous species II even further, which would increase k_{cat}, opposite of what is observed (Table 1). Therefore, we focus on the reduction potentials of the three enzymes as the principle contribution to the change in rate of catalysis. Reducing the donor ability of the varied ligand on the iron should destabilize the oxidized site more than the reduced site and raise $E°$. For WT SLO-1, EPR studies show that the interaction of the Asn ligand with the ferric ion is very weak (i.e., axial EPR signal, $E/D = 0.01$). The interaction increases with N694H SLO-1 ($E/D = 0.08$) and is strongest with the 15-HLO, based on its rhombic limit EPR signal ($E/D = 0.33$). Thus, one would expect the ferric site in WT SLO-1 to be easiest to reduce (highest $E°$, >600 mV[39]), and this would decrease down the LO series, with 15-HLO having the lowest $E°$. This trend in $E°$ can be estimated from the change in energy of the His-to-Fe^{3+} charge-transfer band in the CD spectrum (Figure 6). LMCT bands reflect the reduction potential of the iron, as the ligand orbital being oxidized is approximately fixed in energy for a given ligand. The LMCT band (Figure 6) is found to be at higher energy for N694H SLO-1 (∼400 nm (25 000 cm^{-1})) as compared to WT SLO-1 (∼425 nm (23 800 cm^{-1})), signifying a shift to lower reduction potential ($E°$) for N694H SLO-1. Thermodynamic calculations show that this increase in the LMCT band energy correlates to a ∼100 mV change in $E°$. This is roughly equivalent to 1.7 units in pK_a for the water in the reduced species II in its contribution to the strength in the O−H bond. This is consistent with the former being the dominant contribution to the hydrogen atom abstraction driving force, since the latter is already very high (pK_a > 11.5) in WT SLO-1. A decrease in reduction potential by 100 mV would decrease k_{cat} by a factor of ∼50, which is consistent with the fact that the k_{cat} of N694H SLO-1 is 28 times lower than that of WT SLO-1.

(37) The KIE data were obtained using a novel, competitive RP-HPLC method (submitted for publication).

(38) Gardner, K. A.; Mayer, J. M. *Science* **1995**, *269*, 1849−1851.

(39) Nelson, M. J. *Biochemsitry* **1988**, *27*, 4273−4278.

Our studies indicate that the extent of the Fe^{3+} rhombicity correlates with reactivity by reflecting the increased interaction of the axial ligand with the ferric site which stabilizes this oxidation state, lowering the redox potential, and thus acting as the driving force for hydrogen atom abstraction. We are now in the process of systematically mutating this Asn ligand position to other amino acids to vary the coordination interactions with the ferric and ferrous sites and to correlate this with their reactivity. This should provide significant molecular-level insight into factors which control the lipoxygenase catalytic mechanism.

Acknowledgment. This research was supported by the National Institutes of Health (E.I.S., GM40392; T.R.H., GM56062-01). Thanks is given to David Sloane, Michael Hendrich, and Elizabeth G. Pavel for helpful discussions, Bernard Axelrod for determination of the 13-(*S*)-HPOD chirality, Eric Johansen for technical support, and Glenn Millhauser for the use of the EPR spectrometer. T.R.H. also gratefully acknowledges the generous financial support of the Helen Hay Whitney Foundation, Dr. Elliott Sigal (NIH), the UC Riverside Chemistry Department, and the Petroleum Research Fund (ACS-PRF 30984-G3).

Supporting Information Available: The near-IR MCD (5 K, 6 T) spectra of ferrous WT SLO-1 at pH = 7, 9, and 11 in glycerol, showing no pH-dependent spectral changes (1 page). See any current masthead page for ordering information and Web access instructions.

JA982844C